Contrasting fire damage and fire susceptibility between seasonally flooded forest and upland forest in the Central Amazon using portable profiling LiDAR

Article *in* Remote Sensing of Environment · October 2016

DOI: 10.1016/j.rse.2016.06.017

CITATIONS
34

READS
491

7 authors, including:

Danilo Roberti Alves de Almeida
University of São Paulo
52 PUBLICATIONS **274** CITATIONS

SEE PROFILE

Bruce Walker Nelson
Instituto Nacional de Pesquisas da Amazônia
129 PUBLICATIONS **8,697** CITATIONS

SEE PROFILE

Juliana Schietti
Federal University of Amazonas
95 PUBLICATIONS **3,000** CITATIONS

SEE PROFILE

Eric Bastos Gorgens
Universidade Federal dos Vales do Jequitinhonha e Mucuri
92 PUBLICATIONS **445** CITATIONS

SEE PROFILE

Remote Sensing of Environment 184 (2016) 153–160

Contents lists available at ScienceDirect

Remote Sensing of Environment

journal homepage: www.elsevier.com/locate/rse

Contrasting fire damage and fire susceptibility between seasonally flooded forest and upland forest in the Central Amazon using portable profiling LiDAR

Danilo Roberti Alves de Almeida [a,*], Bruce Walker Nelson [a], Juliana Schietti [a], Eric Bastos Gorgens [b], Angélica Faria Resende [a], Scott C. Stark [c], Rubén Valbuena [d]

[a] INPA - Brazil's National Institute for Amazon Research, Av. André Araújo, 2936, 69067-375 Manaus, AM, Brazil
[b] USP/ESALQ, University of São Paulo, Av. Pádua Dias, 11, 13418-900 Piracicaba, SP, Brazil
[c] Department of Forestry, Michigan State University, East Lansing, MI 48824, USA
[d] University of Eastern Finland, Faculty of Forest Sciences, PO Box 111, Joensuu, Finland

ARTICLE INFO

Article history:
Received 11 November 2015
Received in revised form 5 June 2016
Accepted 22 June 2016
Available online xxxx

Keywords:
Forest fire
Amazon
Leaf area profiles
Remote sensing of canopy structure
LiDAR
Structural attributes
Leaf area density
Igapó
Floodplain forest
Terra firme

ABSTRACT

Fire is an increasingly important agent of forest degradation in the Amazon, but little attention has been given to the susceptibility of seasonally flooded forests to fire. Satellite images suggest that forests flooded seasonally by nutrient-poor black waters are more susceptible to fire and may suffer greater fire damage than nearby upland forests. Reasons for this difference may include the presence of a root mat, more fine fuel as litter and a drier understory in the flooded forest. We investigated this difference in the field, hypothesizing that differences in the aboveground structure of the pre-burn forest can contribute to the difference in impacts of, and susceptibility to, fires. We employed a portable profiling LiDAR (PPL), first to compare damage between adjacent black water seasonally flooded and upland forests that were burned by the same fire event, and to then assess pre-fire canopy structure attributes known to affect fire susceptibility. For both assessments, we used PPL-derived metrics of leaf area and vertical and horizontal variation in the structure of vegetation in the canopy. Four years after the fire, the LiDAR metrics showed greater combined effects of high damage and slow recovery in the seasonally flooded forest; reduction of total Leaf Area Index (LAI) after burning was only 10% for upland forest but was 71% in the flood forest. Compared to unburned upland, the canopy of unburned flood forest had structural differences that increase susceptibility to fire, including drier microclimate. It had more gaps, a more open understory and a lower upper canopy. Small patches lacking canopy closure (LAI < 1.0) were far more abundant in the unburned flood forest. We conclude that black water seasonally flooded forest suffers greater fire damage than upland forest and canopy structure contributes to its greater susceptibility to the occurrence of fires. This must be considered in assessments of future Amazon fire risks and impacts, including flood forest acting as a potential conduit for spreading fire to upland forest.

1. Introduction

Tall and dense mature forests of Amazon upland (*terra firme*) are resistant to drought and to the penetration of surface fire. Deep shade of the understory, with few gaps, maintains high relative humidity, reducing the possibility of fire ignition (Ray, Nepstad, & Moutinho, 2005; Uhl, Kauffman, & Cummings, 1988), while rapid decomposition of litter keeps fine fuel stock low (Martius, Höfer, Garcia, Römbke, & Hanagarth, 2004). In contrast, Amazon upland forests that have suffered structural damage by mechanized logging and/or by a recent fire are vulnerable to recurring fire (Cochrane et al., 1999; Nepstad et al., 2001), especially in drought years (Alencar, Asner, Knapp, & Zarin, 2011). Logging and prior fire disturbance increase coarse and fine fuel loads on the ground and open large sunlit gaps, leading to hotter temperatures and lower relative humidity (Holdsworth & Uhl, 1997; Ray et al., 2005). When the understory relative humidity is <65%, litter layer fine fuel becomes vulnerable to ignition (Uhl et al., 1988).

Forests flooded annually by nutrient-poor acid black waters (*igapó*) suffer much greater post-fire impact than do upland forests (Flores, Piedade, & Nelson, 2012; Nelson, 2001). The difference in fire damage between these two widespread (Melack & Hess, 2010) Amazon forest types has, however, only recently been compared under identical recent precipitation history and similar proximity to ignition sources (Resende, Nelson, Flores, & Almeida, 2014). Very low tree growth and recruitment rates in black water flood forests (Junk et al., 2011) delay post-fire

* Corresponding author.
E-mail address: daniloflorestas@gmail.com (D.R.A. Almeida).

http://dx.doi.org/10.1016/j.rse.2016.06.017
0034-4257/

succession. Black water flood forests burned in 1926 and 1997 remained dominated by open non-woody vegetation in 2010 (Ritter, Andretti, & Nelson, 2012; Williams et al., 2005).

When compared in the dry season to nearby upland forest, the black water flood forest has a greater accumulation of fine combustible leaf litter above the ground and a thicker mat of combustible fine tree roots, just below the litter and above the mineral soil. Both are a consequence of slow leaf decomposition under water (Dos Santos & Nelson, 2013; Kauffmann, Uhl, & Cummings, 1988). During the late dry season, the now exposed litter and fine root mat of the black water flood forest become dry and flammable after just nine days without rain (Uhl et al., 1988). Furthermore, black water flood forests appear to have more open space in their canopy and understory, which would permit greater airflow. Together with the greater fine fuel and higher ignition risk environments of black water flood forest during dry conditions, this may increase the probability of fire spread relative to adjacent upland forest. Once a fire has initiated in flood forest, local residents report that a low intensity smoldering ground fire, similar to a peat fire, burns the root mat and causes high tree mortality.

As an indicator of susceptibility to fire establishment, Resende et al. (2014) compared the microclimate near the litter layer in unburned black water flood forest, at low water stage in the late dry season, to the litter layer microclimate in adjacent unburned upland forest. They found lower extremes of relative humidity and higher temperature extremes in the flood forest. They then compared post-fire damage between the two forest types, taking advantage of a natural experiment: the same fire event penetrating both forest types. Comparing replicate unburned and burned plots of each forest type, post-fire losses of basal area and stem density were highest in the seasonally flooded forest. However, forest structure attributes known to affect fire susceptibility were not measured or compared between the two pre-burn forest types.

Lower canopy height, lower leaf area index (LAI) and more canopy gaps are three canopy structure attributes known to increase the probability of ground fire establishment. Ray et al. (2005) have shown that, when controlling for recent rainfall history and for the microclimate and the wind velocity outside of different upland forests, the understory relative humidity decreases and fire spread rate increases with lower canopy height and lower LAI. Daytime relative humidity near the litter layer is lower in gaps where sunlight penetrates to ground level (Holdsworth & Uhl, 1997) and low humidity is a strong predictor of fire spread rate (Ray et al., 2005).

Here we expand on the work of Resende et al. (2014), using new data for the burned and unburned black water flood and upland forest plots of that Central Amazon study. Aboveground structural attributes were measured with a portable profiling LiDAR (PPL) (Parker, Harding, & Berger, 2004; Stark et al., 2012). These were compared between burned flood and upland forest plots to assess damage differences, and then compared between unburned plots of both types for the canopy attributes known to increase fire susceptibility. We examine three hypotheses:

(1) Fire impacts are higher in black water flood forests. Pre- to post-fire change in canopy height, canopy openness and LAI will reveal greater aboveground structural damage in the flood forest;
(2) Compared to unburned upland forest, unburned black water flood forest will have structural differences previously shown to increase susceptibility to fire establishment and spread. These include lower canopy height, higher gap fraction and lower LAI;
(3) We also hypothesized that PPL metrics may provide useful predictions of indicators commonly used to quantify fire damage severity: basal area (BA) and stem density (SD) loss. This hypothesis was motivated by prior foundational studies showing potential relations between PPL and forest parameters (Parker et al., 2004; Stark et al., 2015) and successful predictions for biomass growth (Stark et al., 2012).

2. Material and methods

2.1. Field site

Fire scars are common in the forests of the floodplain of the Rio Negro, the world's largest black water river, but few sites present a natural experiment where nearby upland and seasonally flooded forests were impacted by the same fire. We used a time series of Landsat Thematic Mapper satellite images to identify a field site 100 km south of Manaus (Figs. S1, S7), centered at 03°43′ S and 60°14′ W, where these two forest types were intercalated and burned only once, in November of 2009, during an El Niño-related drought. A burn severity map of the study region, based on pre- to post-fire change in the Normalized Burn Ratio (delta-NBR), suggested differential damage in the two forests types when exposed to the same fire event (Fig. S1). For reasons described in Supplementary Text 1, it is clear that forest damage at our site was caused by the 2009 fire and not directly by drought, nor by the record low water levels of 2010 (Marengo, Tomasella, Alves, Soares, & Rodriguez, 2011). Among these is the fact that forest damage occurred on only one side of the line of maximum fire advance (Fig. S1a) and that the post-burn image for the fire damage map (Fig. S1b), was from a date well before the extreme low water levels of 2010.

We distributed ten burned and ten unburned plots of each forest type, seasonally flooded and upland, on opposing sides of the line of maximum fire advance (Figs. S1, S2, S8 and S9). Each of the 40 plots was 0.5 ha in area, 250 m long by 20 m wide. We spread plots evenly on the unburned side of the fire line. On the burned side, plots were spread over a similar area and evenly within two groups, due to landholder permissions. Black water flood forest here is dry in the late dry season to early rainy season, from October to January. Seasonally flooded forest is restricted to the upper half of the annual flood range, which conveniently minimized the effect of inundation duration on forest structure and composition across all flood forest plots. More site details are provided by Resende et al. (2014).

Conventional inventories provided the basal area and the stem density per plot for all trees over 10 cm diameter at breast height (DBH). These were conducted 3–4 years after the fire. This was sufficient time for delayed fire-related tree mortality to more fully accrue (Barlow, Peres, Lagan, & Haugaasen, 2003), but insufficient time for post-fire regrowth to reach the minimum DBH of 10 cm. Two-dimensional LiDAR profiles of the canopy were collected along the center line of each plot in a single month, November 2013, to avoid any seasonal changes in leaf amount (Haugaasen & Peres, 2005). From these profiles we extracted structural metrics to compare the forest types, related to fire damage and to fire susceptibility. The forest canopy is here defined as all vegetation >1 m above the ground, which is the height of the instrument.

2.2. LiDAR data collection and analysis

The canopy profiling system employs a range-finder type laser, model LD90-3100VHS-FLP manufactured by Riegl (Horn, Austria). Laser wavelength is 900 nm, strongly reflected by vegetation. The distance measurement accuracy is ±25 mm and the nominal range is 200 m without a target plate. The instrument is held in a portable gimbaled structure that maintains vertical aim. A small 12 v battery and a water-resistant computer complete the PPL system (Fig. S3). The operator walks at a constant pace along the plot center line, controlling his speed with the aid of an electronic metronome and markers spaced every two meters. Each of 2000 pulses per second is recorded in an alternating sequence as either a height to the first (1000 pulses) or last (1000 pulses) reflecting object or as a non-returning "sky shot". The latter is useful to measure canopy openness. Raw pulse returns can be plotted as a side-view profile of 250 m length, with sky shots coded as zero height (Fig. S4).

The lidar beam has an oval footprint that, in push broom fashion, samples about 4% of each 1 m deep (across-track) voxel at 5 m height

in the forest and about 11% at 25 m height in the forest. Though only these fractions of each voxel are sampled, there is an empirical relationship between leaf area density of the entire voxel and the data we obtain from the LiDAR for estimating an effective leaf area density (SC Stark, unpublished). The effective LAD of each 2 m along track by 1 m high by 1 m deep cell in a column of voxels is derived from the occlusion rate of pulses reaching that voxel. Some of the pulses entering the voxel are reflected and recorded as returns by the LiDAR while others continue in their path upward to sample further voxels. The ratio of pulses departing to pulses entering each voxel provides a measurement of the absorbance of vegetation within the voxel when it is transformed logarithmically, from which we estimate leaf area density. Voxels that receive <100 input pulses were filtered, to eliminate a bias that creates higher than expected LAD in these voxels (see Discussion). The calculation, provided by MacArthur and Horn (1969), is shown by Eq. (1):

$$\text{Effective LAD} = -\ln(\text{pulses.out}/\text{pulses.in}) \times \frac{1}{D} \times \frac{1}{K}, \quad (1)$$

where Effective LAD is the estimated leaf area density of one voxel in a stack; "pulses.in" is the number of pulses which strike the bottom of the voxel; "pulses.out" is the number of pulses that come out at the top of that voxel; D is the height of the voxel. The second term (1/D) cancels in the case of this study because a voxel height is one meter. The constant K describes the change in absorbed pulses as leaf density increases. K remains constant if all of the following remain fixed: LiDAR beam width, pulse intensity, pulse wavelength, distribution of leaf blade angles and degree of clustering of leaves. Prior studies have assumed K = 1 (Parker et al., 2004; Sumida et al., 2009). Recent work (Stark et al., 2012, 2015; SC Stark, unpublished) also found that K was close to 1 for the same instrument used here, so the third term (1/K) can reasonably be discounted for the purpose of this study.

At the slow walking speed of the operator, we obtained ~14,000 "first plus last" returns in each two-meter along-track section of transect. From these data we extracted estimates of effective leaf area density (LAD) and effective leaf area index (LAI) for each two-meter along-track voxel column (Parker et al., 2004; Stark et al., 2012). For brevity, we hereafter we refer to these estimates as simply LAD and LAI. Leaf clusters, occluded leaves and non-random leaf angle distributions are sources of potential error and bias using the PPL, as is the case with other indirect estimates of LAD or LAI.

The 125 two-meter along-track columns of voxels comprise a two-dimensional side view LAD "image" above a plot's centerline (Fig. S6). The horizontal average at each one meter height level across the 125 columns provides a graph of LAD against height – an LAD estimate with confidence intervals at each 1 m elevation increment. The sum of all horizontal averages provides the average LAI of the transect. Because each voxel's LAD is based on the percent of incoming laser pulses that are returned to the detector, results are independent of operator walking speed during sampling, though we standardized to a slow walking pace for a high return density.

2.3. Testing the hypotheses

To test our first hypothesis, that LiDAR derived metrics of canopy structure detect greater pre- to post-fire canopy structure damage in the black water seasonally flooded forest, we compared post-burn change of an attribute for each forest type (n = 10 per type), relative to a single pre-burn proxy value for that attribute, which was the average value of the ten unburned plots of that forest type. Hereafter, where we describe pre- to post-burn damage, loss or change in a forest structure attribute we are always referring to this pre-burn proxy. This is the case for the LiDAR-derived and for the inventory derived attributes (basal area and stem density). Differences between burned upland and burned flood forests were evaluated in terms of their respective changes using Mann-Whitney *U* tests. Attributes whose fire-caused changes were compared between the two forests are (1) total LAI, (2) LAD within the understory 1–4 m above the ground, (3) top-of-canopy height, (4) canopy openness above 15 m height and (5) canopy openness above 1 m height.

For analyses that required LAD or LAI, to increase the pulse number and minimize the effect of filtering voxels with fewer than 100 input pulses, we used two-meter along track segments, thereby providing 14,000 initial pulses per segment. For those attributes that use raw LiDAR returns, we used one-meter along track segments and filtered spurious high returns. We calculated top-of-canopy height as the average of the 250 highest raw laser returns, one from each along-track section (Fig. S5). We obtained two measures of canopy openness. The first is the fraction of the one-meter sections of a plot transect that had no canopy above 15 m height (Fig. S5). This is the canopy gap fraction as defined by Runkle (1982). A 15 m cutoff provides an indication of long-term gap formation rate, as it includes gaps now in their early to middle stages of regeneration. For the second measure of canopy openness we used the percentage of all pulses per transect that were "sky shots", i.e., that did not return from the canopy above the instrument, which was 1 m above the ground.

To test our second prediction, that canopy structure differences between unburned upland and black water flood forest increase fire susceptibility in the latter, we obtained the three structural attributes previously shown to affect fire susceptibility – LAI, canopy height and canopy openness – and compared them between these two unburned forest types. We used two measures of canopy openness, described above. We also used two measures of LAI, one being the average LAI at the plot scale and the other being the fraction of two-meter segments per plot that lacked "canopy closure" (LAI < 1.0). We also compared understory LAD, due to the expected fire quenching by green leaves near the litter layer. LAI and LAD were obtained as described above (Stark et al., 2012, 2015).

To test our third hypothesis, we modeled the relationships between four LiDAR-derived attributes in burned forests ($\boldsymbol{X}$) and the basal area loss and stem density loss ($\boldsymbol{Y}$), using the most similar neighbor method (MSN; Moeur & Stage, 1995). The four LiDAR attributes in ($\boldsymbol{X}$) for each of the two burned forest types were LAI loss (%), canopy height, sky shots and gap fraction at 15 m. MSN is a type of estimation technique within the group of non-parametric imputation methods called the nearest neighbor (*k*-NN), in which a value of $\boldsymbol{Y}$ is predicted for an area of unknown value based on a comparison of its values in the LiDAR metrics (a.k.a. feature space) against those from reference sample plots (McRoberts, Nelson, & Wendt, 2002; Mäkelä & Pekkarinen, 2004). In *k*-NN, distances are measured in the feature space ($\boldsymbol{X}$) to search for the *k* nearest neighbors, whose $\boldsymbol{Y}$ is used for computing a prediction ($\boldsymbol{Y}$) by inverse distance-weighted averaging (Franco-Lopez, Ek, & Bauer, 2001; McInerney, Suárez, Valbuena, & Nieuwenhuis, 2010). The MSN method applies *k*-NN using components from canonical correlation analysis (CCA) as the feature space (Packalén & Maltamo, 2008). This modelling approach was chosen because it can perform well with low sample sizes and non-linear relationships (Valbuena, Vauhkonen, Packalen, Pitkänen, & Maltamo, 2014). The input values were the mean of the responses ($\boldsymbol{Y}$) for the $k = 3$ nearest neighbors, weighted by the inverse of their distances. The value of $k = 3$ was kept low due to the small sample size available since, although a higher *k* may improve the precision of the estimation, it can also bias extreme values toward the average (Eskelson et al., 2009).

2.4. Accuracy assessment

Jack-knife cross-validation was carried out to assess accuracy of the MSN analysis. Thus, after removing one case (i) from the total n, the remaining cases were used to calculate the *k* nearest neighbors and predict the response for that given case (pre_i). The result was evaluated

with observed versus jack-knife predicted plots, from which we evaluated:

(1) the *bias*, considered as the difference between the means of the predicted minus the observed:

$$bias = \overline{pre} - \overline{obs}; \quad (2)$$

(2) the *precision* of the prediction, considered as the root mean squared deviation (*RMSD*) of predicted values with respect to the observed ones (Piñeiro, Perelman, Guerschman, & Paruelo, 2008):

$$RMSD = \sqrt{PRESS/(n-1)}, \quad (3)$$

where *PRESS* was the predicted sum of squares obtained by the cross-validation:

$$PRESS = \sum_{i=1}^{n} (pre_i - obs_i)^2, \quad (4)$$

(3) the *overall agreement*, for which we computed Willmott's (1982) index of agreement (*d*)

$$d = 1 - \left[PRESS / \sum_{i=1}^{n} \left(\left| pre_i - \overline{obs} \right| - \left| obs_i - \overline{obs} \right| \right)^2 \right], \quad (5)$$

which can be interpreted as a coefficient of determination, while being more appropriate for comparing observed versus predicted values (Yebra & Chuvieco, 2009);

(4) the *degree of over-fitting* to the sample, which we estimated from the ratio between the sums of squares obtained in the cross-validation (*PRESS*) versus using the whole dataset (Valbuena et al., 2013):

$$q\text{-}value = \sqrt{PRESS}/\sqrt{SS}, \quad (6)$$

where *SS* was the sum of squares of the model residuals (*j*), i.e. the values fitted from the whole dataset (without cross-validation):

$$SS = \sum_{j=1}^{n} \left(pre_j - obs_j \right)^2; \quad (7)$$

Weisberg (1985) advised not to exceed $q - value = 1.1$, i.e. the real precision should not be >10% of the model residuals.

3. Results

3.1. Pre- to post-fire change

Consistent with our first hypothesis and corroborating the burn severity map (Fig. S1), four LiDAR-derived metrics showed much greater pre- to post-fire change in the black water flood forest. These were the top-of-canopy height, canopy openness viewed from the ground (sky shots), understory LAD at 1–4 m height and full-profile LAI (Table 1). Top-of-canopy height decreased after burning by 44% in the flood forest but only by 12% in upland forest ($p = 0.007$; Table 1, Fig. 1A). Sky shots increased significantly after burning in both forests, indicating an increase in canopy openness, but in burned flood forest this increase was almost thirteen times greater than burned upland forest ($p = 0.001$; Fig. 1B, Table 1). Reduction of total LAI after burning was only 10% for upland forest but was 71% in the flood forest ($p = 0.001$; Table 1, Fig. 1D, Fig. 2).

There was a large loss of vegetation along the entire vertical profile of burned seasonally flooded forest (Fig. 2). In upland, incipient (3–4 year old) post-burn regrowth caused an increase of 52% in the leaf area density in the understory, from 1 to 4 m height (Fig. 2), whereas floodplain lost 59% of its understory leaf area density, a significant difference between the two forests´ net effects of post-burn damage and post-burn recovery ($p = 0.001$, Table 1). Above 12 m height (i.e. above new post-fire regrowth in the upland forest profile) there was a loss of leaf area density in upland forest. This was sufficient to cause a small but significant 10% loss of LAI for the full profile after burning upland forest (Fig. 1D, Fig. 2).

3.2. Differences in structural attributes between unburned upland and flood forests

The three structural attributes previously shown to affect fire susceptibility (Holdsworth & Uhl, 1997; Ray et al., 2005; Uhl et al., 1988) were different in the direction of higher susceptibility in the unburned black water flood forest compared with the unburned upland forest (Table 2). First, the 250 highest laser return heights per transect were, on average, 15% lower in unburned flood forest than in unburned upland forest ($p = 0.001$; Fig. 1A, Table 2). Second, the two indicators of canopy openness were higher in the unburned flood forest. This forest had two times higher gap fraction above 15 m height ($p = 0.001$; Fig. 1C, Table 2) and had three times more sky shots ($p = 0.001$ Fig. 1B, Table 2), suggesting that more direct sunlight reaches the litter layer near local noon. Third, patches of low LAI were more common in the flood forest. At the scale of the 2 m-wide voxel stacks, there was more forest area lacking canopy closure (LAI < 1.0) in unburned flood forest. Specifically, 4.2% of the unburned flood forest's area lacked canopy closure, whereas only 0.4% of the unburned upland forest area lacked canopy closure (Table 2). At the plot scale of 250 m, however, LAI did not differ significantly between the two unburned forest types ($p = 0.43$; Table 2, Fig. 1D).

The two forests had different vertical distributions of leaf density (Fig. 3). Unburned flood forest had about half the vegetation density close to the litter layer, from 1–4 m ($p = 0.001$; Table 2), where green leaves can contribute to fire quenching. Above 22 m the leaf density was also much lower in the flood zone ($p = 0.002$; Table 2), consistent with that forest having a generally shorter canopy. From 4 to 22 m, flood forest LAD was, on average, denser than the upland ($p = 0.004$; Table 2), but this average does not portray the fact that LAI was more spatially variable at the small patch scale.

3.3. Predicting fire severity

Regarding our last hypothesis, that PPL metrics obtained in the two types of burned forests may provide reliable predictions of basal area (BA) loss and stem density (SD) loss, to quantify fire damage severity, the diagnosis of the jack-knife predictions obtained by MSN are summarized in Table 3. In both cases, the nearest neighbor imputation method obtained unbiased estimates with residual homoscedasticity. Diagnosis was positive for BA loss. However, the index of agreement for SD loss was very low, and a *q*-value reaching 1.60 was regarded as a sign of

Table 1
Pre- to post-burn percent decrease in five LiDAR metrics. Negative values represent increase. p-Values from Mann-Whitney *U* tests. Metrics are defined in Table 2.

Metric	Burned flood forest		Burned upland forest		p-Value
	Mean	SD	Mean	SD	
LAD (1–4 m)	59%	20%	−52%	38%	0.001
LAI	71%	14%	10%	8%	0.001
Canopy height	44%	24%	12%	11%	0.007
Sky shots (%)	−1282%	396%	−134%	127%	0.001
Gap Fraction (>15 m)	−206%	116%	−166%	114%	0.393

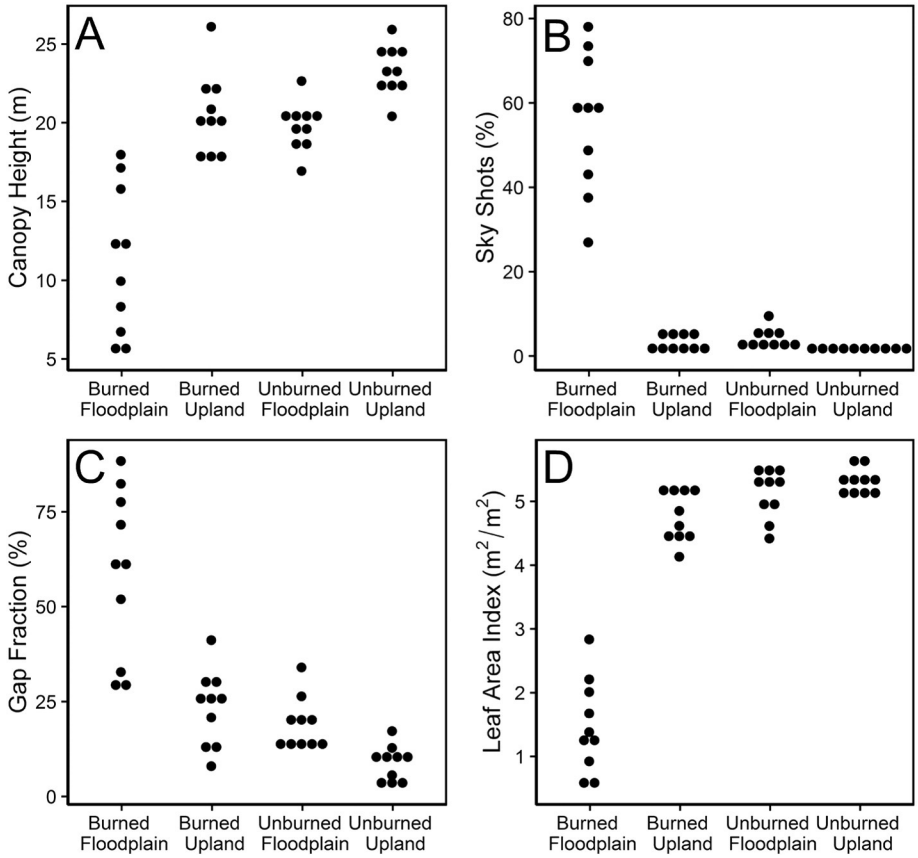

Fig. 1. Dot-density plots, where each dot represents a 250 m transect, for four LiDAR-derived structural attributes of burned and unburned upland and black water flood forests: mean top-of-canopy height (A); Sky shots as a percent of all pulses (B); gap fraction > 15 m height (C); and full-profile LAI (D).

an over-fitted estimation, i.e., the cross-validated errors were 60% larger than the residual variance (q-value > 1.1, Table 3; Weisberg, 1985). The proportion of explained variance in BA loss was 77%, while for SD loss it was only 35%. The uncertainty of the estimation reached 18.0% for BA loss and 29.8% for SD loss.

4. Discussion

4.1. Fire damage and susceptibility

Because both forest types were subjected to the same prior rainfall and were burned by the same fire event, any differences in post-fire damage are due to intrinsic pre-burn characteristics of each forest type. Consequently, greater post-fire damage in flood forest is here taken to indicate greater susceptibility to fire. The pre-burn structural differences identified here are not, however, the only relevant factors. It is not yet possible to partition the relative contributions of pre-burn canopy openness, canopy height, understory density, root mat presence and fine fuel load to the observed fire damage and to the inferred differences in fire susceptibility between the two forest types. However, these factors act in concert and in the same direction, favoring higher fire damage in the flood forest.

In this study we show that pre-burn structural differences assessed with PPL (Table 2) – lower density vegetation in the understory, lower

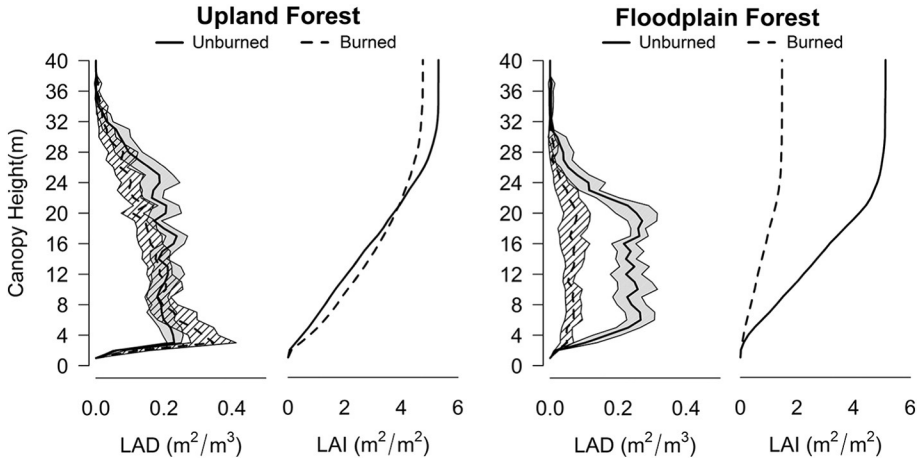

Fig. 2. Leaf area density and cumulative leaf area index profiles comparing burned and unburned plots of the same forest type in each graph.

Table 2
LiDAR-derived metrics of forest structure comparing unburned black water flood and upland forests. p-Values from Mann-Whitney *U* test.

Metric	Unburned flood forest		Unburned upland forest		p-Value
	Mean	SD	Mean	SD	
LAD (1–4 m)	0.29	0.12	0.52	0.08	0.001
LAD (4–22 m)	4.32	0.50	3.59	0.42	0.004
LAD (>22 m)	0.68	0.28	1.37	0.38	0.002
LAI	5.12	0.38	5.31	0.20	0.427
Low LAI area (%)	4.2	3.5	0.4	1.7	0.001
Canopy height (m)	19.8	1.5	23.3	1.6	0.001
Sky shots (%)	4.04	2.64	1.44	0.73	0.001
Gap fraction (>15 m)	0.19	0.07	0.09	0.05	0.001

Where LAD = effective leaf area density; LAI = effective leaf area index; low LAI area = percent of 2 m along-track voxel stacks lacking canopy closure (LAI < 1.0); canopy height (m) = mean of 250 maximum heights per transect; sky shots = percentage of all laser pulses that did not return; gap fraction (>15 m) = fraction of the 250 voxel stacks per transect that had no laser returns above 15 m height.

top-of-canopy height, higher gap frequency and more area lacking canopy closure – are consistent with the drier microclimate in black water flood forest (Resende et al., 2014). Drier microclimate increases the number of days per year that ignition is possible and may contribute to more severe effects of fire. Our results agree with Haugaasen and Peres (2005), who also found higher canopy openness in flood forest compared with upland forest. Higher light penetration, greater openness of the understory, and an open and low upper canopy layer likely lead to higher sensible heat fluxes during the dry season, and may facilitate the penetration of turbulent airflows into the subcanopy and understory (Hutyra et al., 2008). Gaps, specifically, allow higher input of solar radiation to lower layers of the forest (Brokaw, 1985; Holdsworth & Uhl, 1997) and facilitate the occurrence of fire (Ray et al., 2005). Once established, litter layer surface fires are less likely to be quenched given the paucity of living vegetation with green leaves in the flood forest understory (Fig. S8).

Our MSN results suggest that the LiDAR metrics we selected were better able to estimate basal area loss than stem density loss (Table 3). While the MSN method is well-suited for dealing with the low sample sizes, we could not rigorously evaluate the potential of our approach

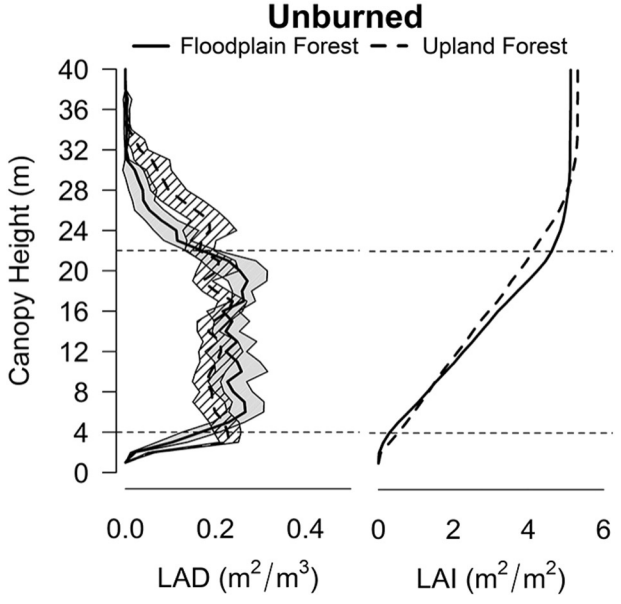

Fig. 3. Leaf area density (±2 SE) along vertical profile (left) and cumulative leaf area index (right) in the unburned black water flood forest (solid lines) and unburned upland forest (dashed lines). The line at 4 m is the top of the understory, From 4–22 m the flood forest has higher leaf density than upland, above 22 m the upland leaf density is higher.

Table 3
Summary diagnosis of most similar neighbor (MSN) predictions.

	Basal area loss	Stem density loss
Bias (cross validated)	−0.005	−0.024
RMSD (cross validated)	0.180	0.298
Index of agreement (*d*)	0.770	0.354
q-Value (over-fitting)	1.071	1.598

for stem density estimation without a higher number of plots. Stark et al. (2015) demonstrated the potential for the prediction of (diameter structured) stem density from LiDAR derived canopy profiles, but also relied on light measurements. They concluded ultimately that plasticity in tree architecture over light is a critical factor influencing the relationship between stand biometric variables (e.g. BA and SD) and vertical canopy structure. An approach taking such plasticity and environmental factors into account could improve prediction of BA and potentially SD in forests impacted by fire, using vertical vegetation profiles obtained by LiDAR.

Damage is not only greater but it also appears to persist longer in black water flood forest than in upland forest. For reasons not yet understood, post-fire succession in black water flood forest is slower than in upland (Flores et al., 2012). At our site, a more rapid filling of the upland understory is evident by comparing pre- and post-burn upland understory LAD in Fig. 2. Burned black water flood forest sites remain dominated for years by low shrubs, forbs, sedges and grasses, all susceptible to reburning (Woods, 1989; Ritter et al., 2012). Oliveira et al. (2014) found an interaction between fire and flooding in reducing the abundance and richness of regenerating plants; fire killed young individuals, while inundation slowed recolonization by tree seedlings.

4.2. Forest structure attributes from LiDAR

The PPL system proved to be effective for evaluating fire damage and susceptibility, providing LiDAR metrics describing fire-relevant structural attributes in the two forests. Rapid and efficient collection of a suite of useful structural attributes using the PPL has been reported in previous studies (Stark et al., 2012, 2015), though this is the first use of this technology for forest fire damage assessment in the Amazon. The instrument and data processing are still being improved. For example, the choice of threshold for filtering voxels with a "low" number of input pulses had a strong effect on the shape of the frequency histogram of LAI classes (Fig. S10). Fortunately, this threshold choice had little effect on relative shape of vertical profiles of leaf area density when comparing the two unburned forests, where profile differences are most subtle.

The PPL has some advantages over airborne LiDAR data; point density is about three orders of magnitude higher and no post-processing is needed to remove ground height. However, only 2D profiles are produced. Problems shared with airborne LiDAR include partial occlusion of the most distant portion of the canopy (upper canopy for PPL, understory and ground for airborne) (Harding, Lefsky, Parker, & Blair, 2001). Occlusion of upper canopy affects estimates of total height, of rugosity and of upper leaf area density (Parker et al., 2004). For both methods, the coefficient K may vary with height in the canopy, forest composition, and light environments. For example, leaf angles change from planophile to random or erectophile with increasing height (e.g., Posada, Lechowicz, & Kitajima, 2009).

We also used hemispherical cameras at ground level and the LAI 2000 (LI-COR Inc., Lincoln, Nebraska, USA), which provide only one LAI value for the whole profile (Richardson, Moskal, & Kim, 2009). For tropical forests, a single measurement of LAI describing the entire vertical profile appears insufficient to explain differences in the microclimate and the fire susceptibility of different forest types. The fine-scale distribution of leaf density in both the vertical and horizontal directions provided by the PPL can also reduce error and bias arising from the spatial

averaging required by other ground-based and airborne LiDAR systems (Sumida et al., 2009, Richardson et al., 2009).

Our MSN results suggest that knowing the vertical distribution of leaf area density may add predictive power for plot-scale estimates. In agreement with this, Stark et al. (2015) have recently shown that LiDAR derived vertical canopy structure metrics can be linked with specific stem size classes to improve the prediction of tree density and basal area, and hence also related size structure indicators (Valbuena et al., 2014). The MSN method was reliable for estimating basal area loss from LiDAR metrics with a limited number of transects, but predicting stem density loss may require a larger sample.

The PPL system shows promise for generating predictive variables for models of fire susceptibility and damage for other tropical forest types, in addition to seasonally flooded black water and upland forests. Vegetation sub-types within the broader "flooded forest" class are in some cases difficult to distinguish (Junk et al., 2011). However, the PPL provides a set of structural characteristics useful to describe and separate these vegetation types and offers potentially explicit links to the estimation of radiation transmission and other ecological variables important to forest function. Further research should focus on using LiDAR – both airborne and ground based – to identify structural differences between floodplain woody vegetation types (Melack & Hess, 2010) and quantitatively link these differences with estimates of the microclimatic variables to rank them according to their susceptibility to fire. This could be useful for recognizing potential hotspots for fire ignition and preventing fire spread to upland forest (Resende et al., 2014).

4.3. Future of black water forests

The role of fire in black water flood forest in the central Amazon has until recently been little studied (Oliveira et al., 2014; Resende et al., 2014) and is little known in wider academic circles. For example, fire was not mentioned in a recent review of threats to Amazonian freshwater ecosystems (Castello et al., 2013). Black water flood forest, however, is here shown to be fragile in the face of forest fires. Fire risk in seasonally flooded forest is important to consider because these forests comprise a large part of the Amazon basin (Melack & Hess, 2010), are adjacent to significant fractions of upland forest (Resende et al., 2014), and serve important roles in environmental services, including in economically important fisheries (Henderson, 1990). This is of particular concern in a world of changing climate. Enhanced drought frequency and intensity, and increasing temperatures in the central Amazon are expected to increase fire broadly and allow fire to spread from disturbed areas into forests that would otherwise resist fire (Aragão et al., 2007; Cochrane & Barber, 2009; Coe et al., 2013; Nepstad et al., 2001).

5. Conclusions

Four years after a fire front passed through adjacent upland and seasonally flooded black water forests, LiDAR metrics showed much higher damage, slower recovery and therefore greater susceptibility to fire in the flood forest. This must be considered when assessing future Amazon fire risks and impacts, including flood forest acting as a conduit for spreading fire to upland forest. While the portable profiling lidar presents significant coverage limitations compared to airborne and orbital sensors due to its 2D profiling nature, it's high pulse density provides fine-scale vertical and horizontal structure of leaf area in the canopy, useful for detecting features related to fire susceptibility.

Acknowledgments

We thank the Amazonas State Foundation for Research Support (FAPEAM 2011 Universal Call) and the Brazilian National Council for Scientific and Technological Development (CNPq process 479722/2012-9) for financial support; the Higher Education Personnel Training Coordination (CAPES) for a student fellowship to DRA Almeida; Bernardo Monteiro Flores for preparing grant proposals; the Study Group on LiDAR technology (Get-LiDAR/ESALQ) for technical assistance in data analysis; Pedro Gama, João Rocha, Aline Lopes and Sebastião Salvino for help in the field; and the Correa and Ribeiro families for authorizing field work on their land. Rubén Valbuena acknowledges support from University of Eastern Finland's strategic funding for the research area of forests, global change and bioeconomy, and a FAPESP travel grant (14/13381-5) for a research visit to Get-LiDAR/ESALQ. SC Stark acknowledges funding support from NSF EF-1340604 and OISE-0730305.

Appendix A. Supplementary data

Supplementary data to this article can be found online at http://dx.doi.org/10.1016/j.rse.2016.06.017.

References

Alencar, A., Asner, G.P., Knapp, D., Zarin, D., 2011. Temporal variability of forest fires in eastern Amazonia. Ecological Applications 21, 2397–2412. http://dx.doi.org/10.1890/10-1168.1.

Aragão, L.E.O., Malhi, Y., Roman-Cuesta, R.M., Saatchi, S., Anderson, L.O., Shimabukuro, Y.E., 2007. Spatial patterns and fire response of recent Amazonian droughts. Geophysical Research Letters 34, L07701. http://dx.doi.org/10.1029/2006GL028946.

Barlow, J., Peres, C.A., Lagan, B.O., Haugaasen, T., 2003. Large tree mortality and the decline of forest biomass following Amazonian wildfires. Ecology Letters 6, 6–8. http://dx.doi.org/10.1046/j.1461-0248.2003.00394.x.

Brokaw, N.V., 1985. Gap-phase regeneration in a tropical forest. Ecology 66, 682–687. http://dx.doi.org/10.2307/1940529.

Castello, L., McGrath, D.G., Hess, L.L., Coe, M.T., Lefebvre, P.A., Petry, P., Macedo, M.N., Renó, F.V., Arantes, C.C., 2013. The vulnerability of Amazon freshwater ecosystems. Conservation Letters 6, 217–229. http://dx.doi.org/10.1111/conl.12008.

Cochrane, M.A., Barber, C.P., 2009. Climate change, human land use and future fires in the Amazon. Global Change Biology 15, 601–612. http://dx.doi.org/10.1111/j.1365-2486.2008.01786.x.

Cochrane, M.A., Alencar, A., Schulze, M.D., Souza, C.M., Nepstad, D.C., Lefebvre, P., Davidson, E.A., 1999. Positive feedbacks in the fire dynamic of closed canopy tropical forests. Science 284, 1832–1835. http://dx.doi.org/10.1126/science.284.5421.1832.

Coe, M.T., Mathews, T.R., Costa, M.H., Galbraith, D.R., Greenglass, N.L., Imbuzeiro, H.M., Levine, N.M., Malhi, Y., Moorcroft, P.R., Muza, M.N., Powell, T.L., Saleska, S.R., Solorzano, L.A., Wang, J., 2013. Deforestation and climate feedbacks threaten the ecological integrity of south-southeastern Amazonia. Philosophical Transactions of the Royal Society, B: Biological Sciences 368, 20120155. http://dx.doi.org/10.1098/rstb.2012.0155.

Dos Santos, A.R., Nelson, B.W., 2013. Leaf decomposition and fine fuels in floodplain forests of the Rio Negro in the Brazilian Amazon. Journal of Tropical Ecology 29, 455–458. http://dx.doi.org/10.1017/S0266467413000485.

Eskelson, B.N.I., Temesgen, H., Lemay, V., Barrett, T.M., Crookston, N.L., Hudak, A.T., 2009. The roles of nearest neighbor methods in imputing missing data in forest inventory and monitoring databases. Scandinavian Journal of Forest Research 24, 235–246. http://dx.doi.org/10.1080/02827580902870490.

Flores, B.M., Piedade, M.T.F., Nelson, B.W., 2012. Fire disturbance in Amazonian blackwater floodplain forests. Plant Ecology and Diversity 7, 319–327. http://dx.doi.org/10.1080/17550874.2012.716086.

Franco-Lopez, H., Ek, A.R., Bauer, M.E., 2001. Estimation and mapping of forest stand density, volume, and cover type using the k-nearest neighbors method. Remote Sensing of Environment 77, 251–274. http://dx.doi.org/10.1016/S0034-4257(01)00209-7.

Harding, D.J., Lefsky, M.A., Parker, G.G., Blair, J.B., 2001. Laser altimeter canopy height profiles: methods and validation for closed-canopy, broadleaved forests. Remote Sensing of Environment 76, 283–297.

Haugaasen, T., Peres, C.A., 2005. Tree phenology in adjacent Amazonian flooded and unflooded forests 1. Biotropica 37, 620–630. http://dx.doi.org/10.1111/j.1744-7429.2005.00079.x.

Henderson, P.A., 1990. Fish of the Amazonian Igapó: stability and conservation in a high diversity-low biomass system. Journal of Fish Biology 37 (Supplement A), 61–66. http://dx.doi.org/10.1111/j.1095-8649.1990.tb05021.x.

Holdsworth, A.R., Uhl, C., 1997. Fire in Amazonian selectively logged rain forest and the potential for fire reduction. Ecological Applications 7, 713–725. http://dx.doi.org/10.1890/1051-0761(1997)007[0713:FIASLR]2.0.CO;2.

Hutyra, L.R., Munger, J.W., Gottlieb, E.W., Daube, B.C., Camargo, P.B., Wofsy, S.C., 2008. LBA-ECO CD-10 Temperature Profiles at km 67 Tower Site, Tapajos National Forest. Data Set. Oak Ridge National Laboratory Distributed Active Archive Center, Oak Ridge, Tennessee, U.S.A., http://www.daac.ornl.gov, http://dx.doi.org/10.3334/ORNLDAAC/863.

Junk, W.J., Piedade, M.T.F., Schöngart, J., Cohn-Haft, M., Adeney, J.M., Wittmann, F., 2011. A classification of major naturally-occurring Amazonian lowland wetlands. Wetlands 31, 623–640. http://dx.doi.org/10.1007/s13157-011-0190-7.

Kauffmann, J.B., Uhl, C., Cummings, D.L., 1988. Fire in the Venezuelan Amazon 1: fuel biomass and fire chemistry in the evergreen rainforest of Venezuela. Oikos 53, 167–175.

MacArthur, R., Horn, H., 1969. Foliage profile by vertical measurements. Ecology 50, 802–804.

Mäkelä, H., Pekkarinen, A., 2004. Estimation of forest stand volumes by Landsat TM imagery and stand-level field-inventory data. Forest Ecology and Management 196, 245–255. http://dx.doi.org/10.1016/j.foreco.2004.02.049.

Marengo, J.A., Tomasella, J., Alves, L.M., Soares, W.R., Rodriguez, D.A., 2011. The drought of 2010 in the context of historical droughts in the Amazon region. Geophysical Research Letters 38, LI2703. http://dx.doi.org/10.1029/2011GL047436.

Martius, C., Höfer, H., Garcia, M.V., Römbke, J., Hanagarth, W., 2004. Litter fall, litter stocks and decomposition rates in rainforest and agroforestry sites in central Amazonia. Nutrient Cycling in Agroecosystems 68, 137–154. http://dx.doi.org/10.1023/B:FRES.0000017468.76807.50.

McInerney, D.O., Suárez, J., Valbuena, R., Nieuwenhuis, M., 2010. Forest canopy height retrieval using Lidar data, medium-resolution satellite imagery and kNN estimation in Aberfoyle, Scotland. Forestry 83, 195–206. http://dx.doi.org/10.1093/forestry/cpq001.

McRoberts, R.E., Nelson, M.D., Wendt, D.G., 2002. Stratified estimation of forest area using satellite imagery, inventory data, and the k-nearest neighbors technique. Remote Sensing of Environment 82, 457–468. http://dx.doi.org/10.1016/S0034-4257(01)00209-7.

Melack, J.M., Hess, L.L., 2010. Remote sensing of the distribution and extent of wetlands in the Amazon basin. In: Junk, W.J., Piedade, M.T.F., Wittmann, F., Schongart, J., Parolin, P. (Eds.), Amazonian Floodplain Forests. Springer, Netherlands, pp. 43–59.

Moeur, M., Stage, A.R., 1995. Most similar neighbor: an improved sampling inference procedure for natural resource planning. Forest Science 41, 337–359.

Nelson, B.W., 2001. Fogo em florestas da Amazônia central em 1997. Proceedings Tenth Brazilian Remote Sensing Symposium. Foz de Iguaçu, 1675–1682 http://www.dsr.inpe.br/sbsr2001/oral/246.pdf Access 04/07/2015.

Nepstad, D., Carvalho, G., Barros, A.C., Alencar, A., Capobianco, P.J., Bishop, J., Moutinho, P., Lefebvre, P., Silva, U.L., Prins, E., 2001. Road paving, fire regime feedbacks, and the future of Amazon forests. Forest Ecology and Management 154, 395–407. http://dx.doi.org/10.1016/S0378-1127(01)00511-4.

Oliveira, M.T., Damasceno-Junior, G.A., Pott, A., Paranhos Filho, A.C., Suarez, Y.R., Parolin, P., 2014. Regeneration of riparian forests of the Brazilian Pantanal under flood and fire influence. Forest Ecology and Management 331, 256–263. http://dx.doi.org/10.1016/j.foreco.2014.08.011.

Packalén, P., Maltamo, M., 2008. Estimation of species-specific diameter distributions using airborne laser scanning and aerial photographs. Canadian Journal of Forest Research 38, 1750–1760. http://dx.doi.org/10.1139/X08-037.

Parker, G.G., Harding, D.J., Berger, M.L., 2004. A portable LiDAR system for rapid determination of forest canopy structure. Journal of Applied Ecology 41, 755–767. http://dx.doi.org/10.1111/j.0021-8901.2004.00925.x.

Piñeiro, G., Perelman, S., Guerschman, J.P., Paruelo, J.M., 2008. How to evaluate models: observed vs. predicted or predicted vs. observed? Ecological Modelling 216, 316–322. http://dx.doi.org/10.1016/j.ecolmodel.2008.05.006.

Posada, J.M., Lechowicz, M.J., Kitajima, K., 2009. Optimal photosynthetic use of light by tropical tree crowns achieved by adjustment of individual leaf angles and nitrogen content. Annals of Botany 103, 795–805. http://dx.doi.org/10.1093/aob/mcn265.

Ray, D., Nepstad, D., Moutinho, P., 2005. Micrometeorological and canopy controls of fire susceptibility in a forested Amazon landscape. Ecological Applications 15, 1664–1678. http://dx.doi.org/10.1890/05-0404.

Resende, A.F., Nelson, B.W., Flores, B.M., Almeida, D.R.A., 2014. Fire damage in seasonally flooded and upland forests of the Central Amazon. Biotropica 46, 643–646. http://dx.doi.org/10.1111/btp.12153.

Richardson, J.J., Moskal, L.M., Kim, S.H., 2009. Modeling approaches to estimate effective leaf area index from aerial discrete-return LIDAR. Agricultural and Forest Meteorology 149, 1152–1160. http://dx.doi.org/10.1016/j.agrformet.2009.02.007.

Ritter, C.D., Andretti, C.B., Nelson, B.W., 2012. Impact of past forest fires on bird populations in flooded forests of the Cuini River in the lowland Amazon. Biotropica 44, 449–453. http://dx.doi.org/10.1111/j.1744-7429.2012.00892.x.

Runkle, J.R., 1982. Patterns of disturbance in some old-growth mesic forests of eastern North America. Ecology 63, 1533–1546. http://dx.doi.org/10.2307/1938878.

Stark, S.C., Leitold, V., Wu, J.L., Hunter, M.O., de Castilho, C.V., Costa, F.R., McMahon, S.M., Parker, G.G., Shimabukuro, M.T., Lefsky, M.A., Keller, M., Alves, L.F., Schietti, J., Shimabukuro, Y.E., Brandão, D.O., Woodcock, T.K., Higuchi, N., Camargo, P.B., Oliveira, R.C., Saleska, S.R., 2012. Amazon forest carbon dynamics predicted by profiles of canopy leaf area and light environment. Ecology Letters 15, 1406–1414. http://dx.doi.org/10.1111/j.1461-0248.2012.01864.x.

Stark, S.C., Enquist, B.J., Saleska, S.R., Leitold, V., Schietti, J., Longo, M., Alves, L.A., Camargo, P.B., Oliveira, R.C., 2015. Linking canopy leaf area and light environments with tree size distributions to explain Amazon forest demography. Ecology Letters 18, 636–645. http://dx.doi.org/10.1111/ele.12440.

Sumida, A., Nakai, T., Yamada, M., Ono, K., Uemura, S., Hara, T., 2009. Ground-based estimation of leaf area index and vertical distribution of leaf area density in a *Betula ermanii* forest. Silva Fennica 43, 799–816.

Uhl, C., Kauffman, J.B., Cummings, D.L., 1988. Fire in the Venezuelan Amazon 2: environmental conditions necessary for forest fires in the evergreen rainforest of Venezuela. Oikos 53, 176–184.

Valbuena, R., Maltamo, M., Martín-Fernández, S., Packalen, P., Pascual, C., Nabuurs, G.J., 2013. Patterns of covariance between airborne laser scanning metrics and Lorenz curve descriptors of tree size inequality. Canadian Journal of Remote Sensing 39 (S1), S18–S31. http://dx.doi.org/10.5589/m13-012.

Valbuena, R., Vauhkonen, J., Packalen, P., Pitkänen, J., Maltamo, M., 2014. Comparison of airborne laser scanning methods for estimating forest structure indicators based on Lorenz curves. ISPRS Journal of Photogrammetry and Remote Sensing 95, 23–33. http://dx.doi.org/10.1016/j.isprsjprs.2014.06.002.

Weisberg, S., 1985. *Applied Linear Regression*. second ed. John Wiley & Sons, New York.

Williams, E., Dall'Antonia, A., Dall'Antonia, V., Almeida, J.M.D., Suarez, F., Liebmann, B., Malhado, A.C.M., 2005. The drought of the century in the Amazon Basin: an analysis of the regional variation of rainfall in South America in 1926. Acta Amazonica 35, 231–238. http://dx.doi.org/10.1590/S0044-59672005000200013.

Willmott, C.J., 1982. Some comments on the evaluation of model performance. Bulletin of the American Meteorological Society 63, 1309–1313. http://dx.doi.org/10.1175/1520-0477(1982)063<1309:SCOTEO>2.0.CO;2.

Woods, P., 1989. Effects of logging, drought, and fire on structure and composition of tropical forests in Sabah, Malaysia. Biotropica 21, 290–298.

Yebra, M., Chuvieco, E., 2009. Linking ecological information and radiative transfer models to estimate fuel moisture content in the Mediterranean region of Spain: solving the ill-posed inverse problem. Remote Sensing of Environment 113, 2403–2411. http://dx.doi.org/10.1016/j.rse.2009.07.001.